Available online at www.sciencedirect.com
ScienceDirect
Theoretical and Applied Fracture Mechanics 49 (2008) 151–157
theoretical and applied fracture mechanics
www.elsevier.com/locate/tafmec

Evaluation of toughness by finite fracture mechanics from crack onset strain of brittle coatings on polymers

J. Andersons [a,*], J. Modniks [a], Y. Leterrier [b], G. Tornare [b], P. Dumont [b], J.-A.E. Månson [b]

[a] Institute of Polymer Mechanics, University of Latvia, Aizkraukles iela 23, Rīga, LV 1006, Latvia
[b] Laboratoire de Technologie des Composites et Polymères (LTC), Ecole Polytechnique Fédérale de Lausanne (EPFL), CH 1015 Lausanne, Switzerland

Available online 4 December 2007

Abstract

Crack onset strain measurements of a confined layer in tension provide the means for layer toughness estimation. The procedure can be simplified if steady-state conditions prevail starting from the commencement of crack propagation, an assumption frequently employed in energy release rate evaluation. It is demonstrated, by numerical analysis of experimental data, that an estimate of the defect size in the film is needed in order to reliably evaluate its fracture toughness from the crack onset strain. Only if microcracks of sufficient size are present in the brittle layer, the steady-state energy release rate at the crack onset strain can be identified with layer toughness. Otherwise, the toughness estimate obtained by such a procedure is likely to be non-conservative.

Keywords: Coating; Polymer film; Crack onset strain; Fracture toughness

1. Introduction

Fracture toughness determination for free-standing submicron thickness films is extremely complicated experimentally, therefore alternative methods are sought, one of them being crack onset strain (COS) measurement for a thin film adhering to a compliant substrate [1]. As the crack propagation usually is unstable, the fracture toughness of the film is further derived by applying finite fracture mechanics (FFM) [2,3]. Namely, if a crack of a well-defined geometry, e.g. a tunneling or channeling crack, appears spontaneously at a given load level (i.e. its propagation is fast and the finer details of crack development are either of no interest or are not possible to follow), then the actual crack growth process, normally the subject of fracture mechanics, can be neglected and the crack appearance treated as a fracture event. FFM implies that the criterion for such a fracture event is as follows: the finite amount of energy (per unit crack area) released by the event should be equal or exceed the critical energy release rate (ERR). Although the term FFM was introduced in [2], the reasoning behind this approach had been applied to constrained fracture problems in a number of studies before [2].

The interpretation of toughness as derived by FFM arguments is discussed in [3,4]. It is claimed that the FFM approach is best applicable to similar fracture events (e.g. progressive cracking); nevertheless, the applicability of FFM has to be verified by comparing of predictions and experimental results. Such verification can be considered as completed for transverse ply cracking of structural, continuous-fiber-reinforced composite laminates as suggested by the successful modeling of crack density evolution with load [4,5]. However, the confined cracking lamina in this case is much more compliant than the constraining plies whereas in thin film/substrate composites the opposite stiffness relation is quite common. Progressive cracking process in stiff coating/compliant substrate systems has been successfully modeled by FFM (see e.g. [6–8]), while less attention is devoted to cracking onset.

Typically, FFM-based deterministic models of progressive cracking yield reasonably accurate results for most of the crack density (CD) range, apart from low CD region down to COS. Applying a probabilistic FFM analysis with

* Corresponding author.
E-mail address: janis.andersons@pmi.lv (J. Andersons).

0167-8442/$ - see front matter © 2007 Elsevier Ltd. All rights reserved.
doi:10.1016/j.tafmec.2007.11.002

random critical ERR (usually complying with Weibull distribution), a reasonable approximation for continuous-fiber-reinforced laminae, remedies this discrepancy (see e.g. [4,9]). It is consistent with probabilistic fragmentation modeling results [10,11] for strength and fracture toughness criteria of cracking. For both criteria, at typical values of the Weibull modulus, the advanced fragmentation stage proceeds in an almost deterministic manner in contrast with the initial, inherently random, cracking stage [10,11].

However, for ceramics, typical materials of hard brittle coatings, the scatter of strength is thought to result from the presence of flaws of various severity (microcracks of different length) in a material with deterministic toughness [12,13]. The evolution of ERR with the coating crack length l has been considered in several works including [14–16]. It is demonstrated that for a perfect coating/substrate adhesion and elastic or elastic–plastic substrate, the ERR is a monotonically increasing function of the crack length up to the steady-state conditions at a crack length λ_{ss}. At $l \geqslant \lambda_{ss}$, ERR reaches its steady-state value, G_{ss}, ceasing to depend on l. Such a character of ERR development leads to an unstable crack propagation in the case of deterministic, constant coating toughness.

Experimental evidence is appearing that coating crack propagation may be more complicated than suggested by the mentioned models; it can involve a quasi-stable growth of cracks within a narrow strain range [17–20]. Such behavior is likely to result from a local, small-scale heterogeneity in the resistance to crack propagation [21] and/or residual stress field [19]. Clearly, toughness characterization of coatings with heterogeneous resistance to cracking should involve description of toughness distribution of the relevant structural elements (e.g. grains and grain boundaries [22]). However, in the following we consider only unstable crack growth in homogeneous coatings, based on the assumptions detailed above.

Note that the ERR determined by FFM, depending on the details of geometry and stress distribution, is either equivalent or close to steady-state ERR when applied to tunneling or channeling cracks. For fiber-reinforced composite laminates with a specific, cross-ply lay-up considered in [4,5] the cracking layer stiffness is lower in the loading direction than that of the constraining plies, hence the steady-state condition for a tunneling crack is reached at a crack length of the order of lamina thickness. Therefore, a defect with dimensions comparable to the lamina thickness, once its propagation is initiated, could be treated as a steady-state tunneling crack. The situation is drastically different for compliant constraining layers; the steady-state crack length can exceed the brittle layer thickness by orders of magnitude depending on stiffness mismatch [14] and yielding of the substrate [15].

This study concerns estimation of the critical ERR of a thin stiff coating adhering to a tough compliant substrate by using channeling COS under tensile loading. The analysis should be useful to predict the influence of factors such as coating thickness, residual stress state, and confinement state (i.e. tunneling vs channeling).

2. Experimental

Silicon nitride (SiN_x) coatings on two different 125 μm thick polyimide foils (Kapton®VN, Dupont, and Upilex S, UBE) were investigated. The foils were annealed at 120 °C for 30 min before deposition. Silicon nitride coatings ranging in thickness from 50 nm to 800 nm were deposited at 200 °C by plasma enhanced chemical vapor deposition (PECVD). The average roughness of the uncoated PI substrates was measured on three 80 μm × 80 μm areas and found to be equal to 11 nm for Kapton VN and 1.2 nm for Upilex S. Both values are small compared to coating thickness, and the corresponding roughness-induced stress concentration in the thin coating are low enough [23] not to influence initiation of damage during loading the coated films detailed in the following.

The in-plane coating residual stress, σ_i, was calculated from the radius of curvature R of the coated foils (the as-received uncoated PI foils were flat), following the analysis of [24]:

$$\sigma_i = -\frac{E_s h_s^2}{6Rh} \tag{1}$$

where E_s is the Young's modulus of the substrate, h_s and h the substrate and coating thicknesses respectively. (Note that the relation above applies only for $h/h_s \ll 1$; see e.g. [25] for various corrections accounting for coating thickness and Poisson's ratio.) Following the usual convention, compressive stresses are taken as negative. The radius of curvature R of the samples was calculated from the maximum deflection of 55 × 6 mm^2 rectangular samples freely supported by two vertical razor blades, using a binocular lens (Olympus SZH).

The Young's modulus of the silicon nitride coatings was assumed to be equal to 100 GPa. This value was measured by nano-indentation of 400 nm thick SiN_x layers deposited on [1 1 1] silicon substrates with the same PECVD apparatus used for the PI substrates. The Young's modulus of the Kapton VN and Upilex S films were found to be equal to 2.4 GPa and 5.4 GPa at room temperature using uniaxial tensile experiments carried out on a UTS load frame. The residual stress evaluated by Eq. (1) is shown in Fig. 1 as a function of coating thickness.

Fragmentation tests [25] were used to investigate damage processes in the SiN_x/PI composites under tensile loading, and, more specifically, the crack onset strain of the nitride layer. In this technique, the evolution of crack patterns in the brittle coating is monitored as a function of the uniaxial tensile load applied to the substrate, in situ in a microscope. The application of a tensile load to rectangular film specimens (50 × 5 mm^2) was achieved with a computer controlled Minimat unit (Rheometric Systems) using a stepper motor for crosshead displacement within 1 μm accuracy. The tensile unit was mounted under

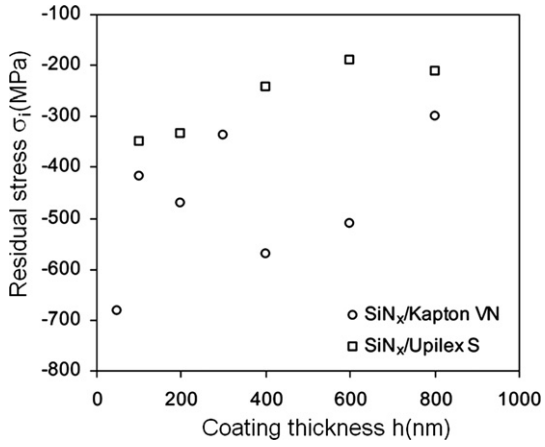

Fig. 1. Residual stress in the coating as a function of the coating thickness for SiN_x/Kapton VN (○) and SiN_x/Upilex S (□).

an optical microscope (Olympus BX60), to allow for magnifications up to 1000×, which provided sufficient resolution for coatings of thickness larger than 50 nm. It was equipped with a coupled-charge device camera (Soft Imaging Systems ColorView II) for non-contact video extensometry of specimen strain with accuracy better than 10^{-4} in strain values [17]. This method eliminated frame compliance and clamp slippage problems. It was verified that the possible influence of ink markers used for extensometry on localized specimen strain was negligible, since their dimension, typically 100 μm, was very small compared to the sample width, equal to 5 mm. Cracking of the coating was analyzed at increasing strain levels in terms of crack density, defined as the inverse of the average fragment length $\langle l \rangle$, and calculated from the average of the number of cracks, N_i, counted on k micrographs of width W, at strain ε, as $\mathrm{CD} = (1+\varepsilon)\sum_{i=1}^{k} N_i/kW$. The factor $(1+\varepsilon)$ corrects for crack opening to a first approximation. The COS was obtained from linear extrapolation of the CD data in the early fragmentation stage, and would in fact correspond to the onset of unstable crack growth.

It was observed that cracks initiated on micron-size defects present in the nitride, such as pin-holes and micro-cracks (so-called macro-defects [26]). The macro-defect population was analyzed using a plasma etching decoration method, in which the coated polymer is exposed to atomic oxygen, and is etched at the location of coating defects [27,28]. This method amplifies the size of defects, which become detectable using optical microscopy, and is a powerful tool to discriminate defects from artifacts such as dust particles. Atomic oxygen etching was carried out for 10 min., on 20 mm^2 circular samples in a Tepla 300 microwave plasma stripper chamber using dual frequency plasma environment under an oxygen pressure equal to 1.275 mbar, with 500 W of power and an oxygen flow rate of 400 ml/min. The optical micrographs reproduced in Fig. 2 show the SiN_x surface, after 10 min exposure to oxygen plasma. The etched undercuts are visible as white, quasi-circular areas, and, in case of Kapton VN, the original defects are visible as a dark spot in the center of the white area. Similar morphologies were observed for the other SiN_x thickness. It is evident that the macro-defect population is markedly different between the two PI substrates: defect sizes are in the range 1–5 μm in case of Kapton VN, and are smaller than 1 μm in case of Upilex S. Fig. 3 shows that the macro-defect density in the coatings decreases with increasing thickness, and that it is systematically lower in case of Upilex S.

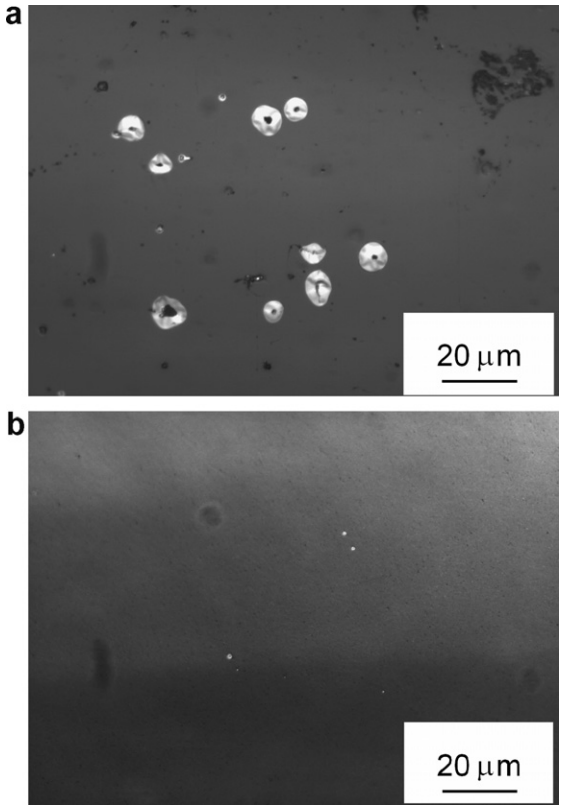

Fig. 2. Morphology of macro-defects in 50 nm thick PECVD SiN_x coatings on Kapton VN (a) and Upilex S (b), revealed by means of atomic oxygen etching method (see text for details).

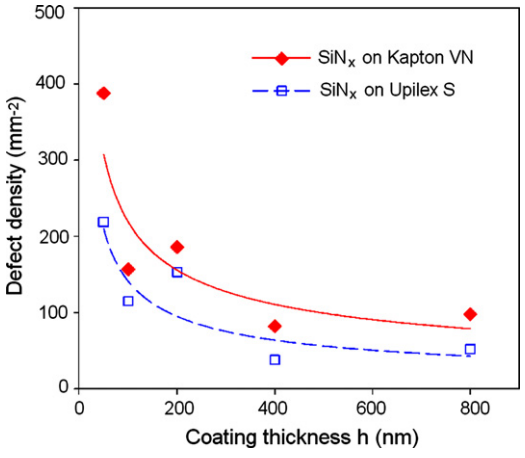

Fig. 3. Macro-defect density in SiN_x coatings of thickness in the range 50–800 nm on PI substrates.

3. Results and discussion

Intrinsic tensile COS (i.e. the strain due to combined action of the applied stress at cracking and the residual stress in the coating) of the SiN_x coating on PI substrates is presented in Fig. 4 as a function of SiN_x layer thickness. The intrinsic COS, $\varepsilon = \varepsilon_a + \varepsilon_i$, is evaluated as a sum of the applied strain at crack onset, ε_a, and the residual strain ε_i. The characteristic scaling of the COS with coating thickness seen in Fig. 4 is in qualitative agreement with FFM that predicts reduction of COS with the increase of coating thickness.

The steady-state ERR attained by a long (with respect to coating thickness) crack corresponds to the FFM estimate of the ERR of a channeling crack. For linear elastic constituents, G_{ss} can be expressed as [29]

$$G_{ss} = \frac{\pi}{2}\frac{\sigma^2 h}{\overline{E}} g(\alpha, \beta) \tag{2}$$

where σ is coating stress, $\overline{E}$ denotes the plain strain modulus of the coating, and $g(\alpha, \beta)$ is a non-dimensional function

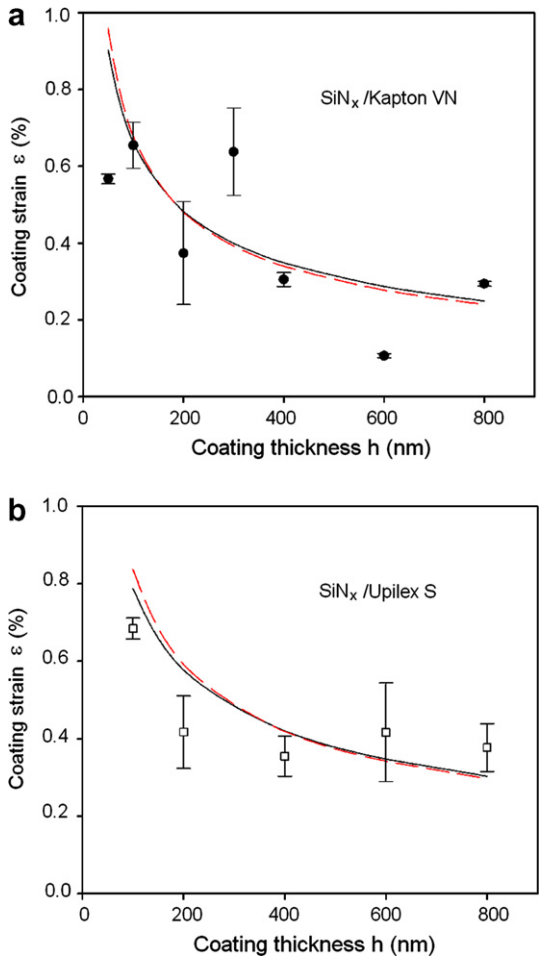

Fig. 4. Coating strain at crack onset vs. coating thickness for SiN_x/Kapton VN (a) and SiN_x/Upilex S (b). Theoretical relation is plotted by dashed line for linear elastic substrate response and by solid line for elastic–plastic response.

of Dundurs' parameters α and β. For SiN_x/Kapton VN the parameter values amount to $\alpha = 0.95$ and $\beta = 0.23$, while for SiN_x/Upilex S they are $\alpha = 0.90$ and $\beta = 0.30$. The function g is evaluated numerically, by 2D model with finite element method (FEM), obtaining $g = 9.1$ and 5.8, respectively, for the mentioned SiN_x/PI systems. The length of a crack, λ_{ss}, at the onset of steady-state condition is estimated as [14]

$$\lambda_{ss} = \pi g(\alpha, \beta) h. \tag{3}$$

Hence, the minimum length of a steady-state crack in SiN_x coating according to Eq. (3) is about $18h$ for Upilex S substrate and $28h$ for the more compliant Kapton VN. The morphological data confirm directly that the steady-state length condition is met for the thinner coatings, as defects of the corresponding size are present in the micrographs taken. The defect size varies considerably, therefore the probability distribution of the maximum defect size in a coating of given area can be derived by the extreme value analysis [30]. Rigorous application of the latter is hampered by the scarcity of defect size measurements for the coatings studied. However, the large number of defects within a typical specimen (given by the product of defect density, Fig. 3, and coating area) and high defect size variability, Fig. 2, indicate that, with high likelihood, coating defects of size λ_{ss} are present also in the medium thickness SiN_x coatings on Kapton VN. The situation is more ambiguous with SiN_x/Upilex S system where defect sizes and density are lower than for SiN_x/Kapton VN (although λ_{ss} is also smaller); nevertheless, it appears reasonable to assume that the steady-state condition for defects is met at least in the relatively thin coatings.

Based on the arguments above, that microcracks of steady-state length (or larger) are indeed present in the coating and develop into channeling cracks at COS, Eq. (2) is applied to evaluate the critical ERR of the coating, G_c, by substituting the coating stress at crack onset for σ in Eq. (2). Thus derived coating toughness estimates are shown in Fig. 5. In the case of Kapton substrate, pronounced scatter of G_c values at different coating thicknesses is seen. By contrast, for Upilex substrate the toughness would appear to slightly correlate with coating thickness. The average coating toughness amounts to 7 J/m^2 for SiN_x/Kapton VN and 6.9 J/m^2 for SiN_x/Upilex S, clearly agreeing within scatter as would be expected.

Although the COS is rather low compared to the yield limit for PI, localized yielding of the substrate is expected at the crack due to high stress concentration. FEM analysis accounting for substrate plasticity according to [31] yielded the average toughness of 12.7 J/m^2 for SiN_x/Kapton VN and 10.5 J/m^2 for SiN_x/Upilex S.

The obtained average toughness value for each SiN_x/PI system is applied for COS prediction with the results shown in Fig. 4. The COS was calculated by substituting the average G_c in the lhs of Eq. (2) for linear elastic substrate behavior, and by iterative FEM analysis for elastic plastic substrate model. The reasonable agreement of theoretical

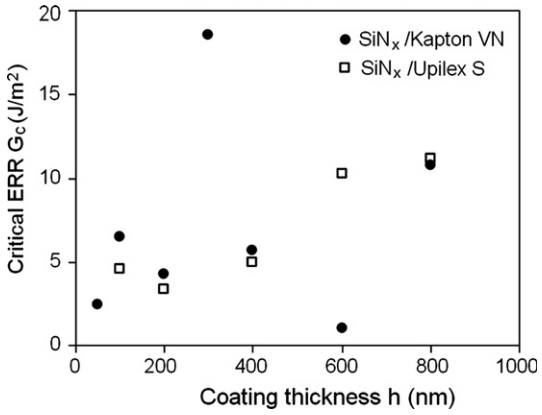

Fig. 5. Critical ERR derived by Eq. (2) using crack onset stress in the coating for SiN_x/Kapton VN (●) and SiN_x/Upilex S (□).

and experimental COS corroborates indirectly the applicability of FFM to the SiN_x/PI systems studied. Furthermore, it also suggests that there is only a weak, if any, dependence of the fracture toughness on coating thickness. It is interesting to note that the presence of localized yielding, while increasing the ERR at COS almost twice, hardly affects the scaling of COS with coating thickness compared to linear elastic substrate response. The scaling of COS $\sim 1/\sqrt{h}$ following from Eq. (2) for elastic response is to be contrasted with the limiting case of perfectly plastic coating/substrate interface that leads to COS $\sim 1/\sqrt[3]{h}$ [32,33].

In several studies [34–36] Eq. (2) has been applied to identify coating toughness from COS data in the case of compliant substrate and reasonable G_c estimates obtained. However, only for ultrathin, 10 nm SiO_x coating considered in [35] the defect size distribution has been determined [23,28]. It has been ascertained that defects of size exceeding the steady-state limit λ_{ss}, Eq. (3), are indeed present. Hence, it is most likely that one of such defects initiated the first crack, in which case Eq. (2) is applicable for the critical ERR estimation as the crack length is above λ_{ss} from the very onset of propagation. It should be noted that, when the length of microcracks present in coating is smaller than λ_{ss}, identifying G_c with the steady-state ERR at COS would lead to a non-conservative G_c estimate.

To exemplify this conclusion, we applied 3D FEM analysis to coating crack onset data for SiO_x/PET obtained at different temperatures and nitrogen atmosphere [37]. The apparent crack onset strain (i.e. the applied mechanical strain) of the $h = 120$ nm coating on 12 μm substrate amounted to $\varepsilon_a = 1.3 \pm 0.1\%$ regardless of the temperature within 26–150 °C range. Yanaka et al. [37] interpreted this result as a proof of strength criterion for coating fracture; this criterion corresponds to the case of crack initiation-controlled failure according to [38,39]. However, the COS data are amenable also to fracture mechanics, i.e. crack propagation-controlled failure analysis presented below.

Using the material data from [37], we performed 3D FEM analysis (accounting for temperature dependence of substrate's elastic–plastic response and the residual stresses) of the cracked coating/substrate system. The FEM model is shown in Fig. 6. The in-plane size of the model was $2000h$ times $2000h$. The crack length was varied from $2h$ to $60h$. Thus the linear dimensions of the model agreed with the convergence condition of 25 times the crack length proposed in [15], apart from the thickness that was limited to the PET film thickness. ABAQUS 20-node quadratic brick elements C3D20 were used. The crack tip was rounded with a radius of $0.0001h$ [15]. First, a temperature loading step was applied in order to obtain the needed level of residual stress, then the model was loaded by displacement (as shown in Fig. 6) up to the prescribed strain. The domain integral method provided by ABAQUS for J integral evaluation was applied with subsequent averaging along the crack front for ERR determination.

The predicted dependence of ERR on coating crack length at the applied 1.3% strain is plotted in Fig. 7. The test temperature clearly has a marked influence on the ERR. Only for 26 °C the steady state is being approached at a crack length exceeding 60 times the coating thickness, the upper limit of crack length chosen for modeling. The trends in Fig. 7 clearly suggest that the steady-state ERR in SiO_x/PET system strongly depends on temperature. Thus the application of FFM approach would produce the apparent SiO_x coating toughness values starting from c.a. 14 J/m^2 at 26 °C and increasing with temperature to over 60 J/m^2.

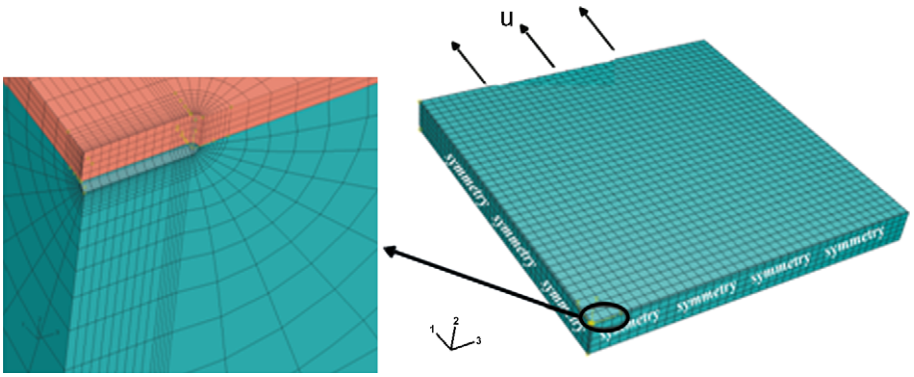

Fig. 6. FEM model for evaluation of channeling crack ERR at different crack lengths.

On the other hand, critical ERR of the SiO_x coating as well as coating defect distribution is highly unlikely to be affected by test temperature. Assuming a plausible value of $G_c = 8\ J/m^2$ and selecting the critical microcrack size of about 1 μm based on the computed ERR, Fig. 7, we further estimated the COS as a function of temperature by FEM. The COS was defined as the applied strain at which the initial microcrack of the given length develops ERR equal to G_c. The results are plotted in Fig. 8 together with the experimental value (dashed line). It is seen that the assumption of a coating defect size being smaller than the steady-state limit provides a reasonably good agreement of the predicted cracking strain with the experimental counterpart.

Thus one can conclude that, in order to reliably identify G_c from COS data, an estimate of the flaw size in the film is needed. Reactive ion etching appears promising as a possible means for accomplishing it in the case of polymer substrates [20,23,27,28]. Alternatively, the coating has to be pre-cracked (see e.g. [40]) thus ensuring that the steady-state conditions apply from the very onset of crack propagation.

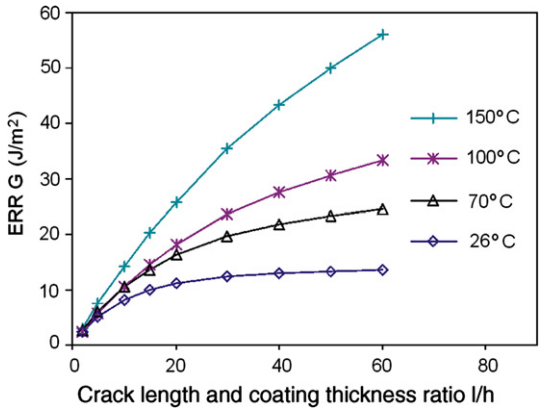

Fig. 7. The development of ERR of a coating crack in SiO_x/PET as a function of temperature and crack length at 1.3% applied strain.

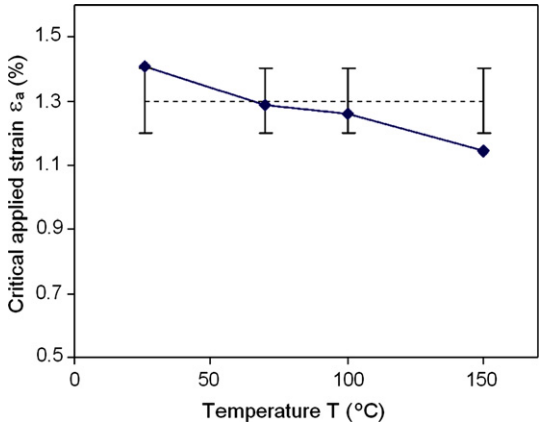

Fig. 8. Experimental [37] (dashed line) and predicted (markers) dependence on temperature of the applied strain at crack onset in SiO_x/PET. The theoretical COS is calculated assuming coating toughness $G_c = 8\ J/m^2$ and the critical microcrack size of 1 μm.

4. Conclusions

The development of fracture pattern in a confined layer under mechanical load reflects both loading conditions and fracture resistance of the layer, thus providing means to probe the properties of the latter. FFM is being successfully used for fracture toughness evaluation from channeling or tunneling CD evolution with tensile load in a confined layer. A deterministic analysis of progressive cracking is usually sufficient as the scatter of local toughness for a fiber-reinforced ply or the variability of microdefect size for a ceramics lamina typically exerts only a minor effect on the advanced fragmentation stage. However, when COS is used for toughness identification of a ceramics layer, an estimate of the flaw size in the film is needed in order to ascertain the applicability of steady-state cracking analysis. Identifying the steady-state ERR at the COS with layer toughness is substantiated if microcracks of such size are present in the brittle layer. Otherwise, it can lead to overestimation of the toughness.

Acknowledgements

The authors gratefully acknowledge the EC 6th framework program for funding this work under contract IST-2004-4354 (FlexiDis). They would like to thank Unaxis Balzers, Display Division for the supply of film samples and Piet Bouten for nano-indentation tests.

References

[1] S. Zhang, D. Sun, Y. Fu, H. Du, Toughness measurement of thin films: a critical review, Surf. Coat. Technol. 198 (2005) 74–84.
[2] Z. Hashin, Finite thermoelastic fracture criterion with application to laminate cracking analysis, J. Mech. Phys. Solids 44 (1996) 1129–1145.
[3] J. Nairn, Applications of finite fracture mechanics for predicting fracture events in composites, in: Fifth International Conference on Deformation and Fracture of Composites, London, 1999, pp. 1–10.
[4] J.A. Nairn, Matrix microcracking in composites, in: A. Kelly, C. Zweben, Eds.-in-Chief. Comprehensive Composite Materials, vol. 2, Pergamon, 2000, pp. 403–432.
[5] J.-M. Berthelot, Transverse cracking and delamination in cross-ply glass-fiber and carbon-fiber reinforced plastic laminates: static and fatigue loading, Appl. Mech. Rev. 56 (2003) 111–147.
[6] C.H. Hsueh, M. Yanaka, Multiple film cracking in film/substrate systems with residual stresses and unidirectional loading, J. Mater. Sci. 38 (2003) 1809–1817.
[7] N.E. Jansson, Y. Leterrier, J.-A.E. Månson, Modeling of multiple cracking and decohesion of a thin film on a polymer substrate, Eng. Fract. Mech. 73 (2006) 2614–2626.
[8] N.E. Jansson, Y. Leterrier, L. Medico, J.-A.E. Månson, Calculation of adhesive and cohesive fracture toughness of a thin brittle coating on a polymer substrate, Thin Solid Films 515 (2006) 2097–2105.
[9] V. Vinogradov, Z. Hashin, Probabilistic energy based model for prediction of transverse cracking in cross-ply laminates, Int. J. Solids Struct. 42 (2005) 365–392.

[10] J. Andersons, Y. Leterrier, G. Tornare, P. Dumont, J.-A.E. Månson, Evaluation of interfacial stress transfer efficiency by coating fragmentation test, Mech. Mater. 39 (2007) 834–844.
[11] J. Andersons, R. Joffe, E. Spārniņš, Statistical model of the transverse ply cracking in cross-ply laminates by strength and fracture toughness based failure criteria, Eng. Fract. Mech., in press, doi:10.1016/j.engfracmech.2007.03.007.
[12] S.B. Batdorf, J.G. Crose, A statistical theory for the fracture of brittle structures subjected to nonuniform polyaxial stresses, J. Appl. Mech. (1974) 459–464.
[13] A.G. Evans, A general approach for the statistical analysis of multiaxial fracture, J. Am. Ceram. Soc. 61 (1978) 302–308.
[14] Z.C. Xia, J.W. Hutchinson, Crack patterns in thin films, J. Mech. Phys. Solids 48 (2000) 1107–1131.
[15] J.M. Ambrico, M.R. Begley, The role of initial flaw size, elastic compliance and plasticity in channel cracking of thin films, Thin Solid Films 419 (2002) 144–153.
[16] J. Andersons, P.H.M. Timmermans, J. Modniks, Mechanics of tunnelling cracks in trilayer elastic materials in tension, Int. J. Fract., submitted for publication.
[17] Y. Leterrier, L. Médico, F. Demarco, J.-A.E. Månson, M. Escola-Figuera, M. Kharrazi-Olsson, U. Betz, F. Atamny, Mechanical integrity of transparent conductive oxide films for flexible polymer-based displays, Thin Solid Films 460 (2004) 156–166.
[18] P.C.P. Bouten, P.J. Slikkerveer, Y. Leterrier, Mechanics of ITO on plastic substrates for flexible displays, in: G.P. Crawford (Ed.), Flexible Flat Panel Displays, John Wiley and Sons, Ltd., 2005, pp. 99–120.
[19] M. George, C. Coupeau, J. Colin, J. Grilhé, Mechanical behaviour of metallic thin films on polymeric substrates and the effect of ion beam assistance on crack propagation, Acta Mater. 53 (2005) 411–417.
[20] S. Grego, J. Lewis, E. Vick, D. Temple, A method to evaluate mechanical performance of thin transparent films for flexible displays, Thin Solid Films 515 (2007) 4745–4752.
[21] J. Andersons, S. Tarasovs, Y. Leterrier, Analysis of thin film cracking and buckling on compliant substrate by fragmentation test, Key Eng. Mater. 348–349 (2007) 329–332.
[22] Y. Charles, F. Hild, On crack arrest in ceramic/metal assemblies, Int. J. Fract. 115 (2002) 251–272.
[23] G. Rochat, Y. Leterrier, L. Garamszegi, J.-A.E. Månson, P. Fayet, Durability of hybrid PECVD-based coatings on semicrystalline polymers, Surf. Coat. Technol. 174 –175 (2003) 1029–1032.
[24] G.G. Stoney, The tension of metallic films deposited by electrolysis, Proc. R. Soc. London A 82 (1909) 172.
[25] Y. Leterrier, Durability of nanosized oxygen-barrier coatings on polymers, Prog. Mater. Sci. 48 (2003) 1–55.
[26] A.P. Roberts, B.M. Henry, A.P. Sutton, C.R.M. Grovenor, G.A.D. Briggs, T. Miyamoto, A. Kano, Y. Tsukahara, M. Yanaka, Gas permeation in silicon-oxide/polymer (SiO_x/PET) barrier films: role of the oxide lattice, nano-defects and macro-defects, J. Membrane Sci. 208 (1–2) (2002) 75–88.
[27] A.S. da Silva Sobrinho, G. Czeremuszkin, M. Latrèche, M.R. Wertheimer, A study of defects in ultra-thin transparent coatings on polymers, Appl. Phys. A 68 (1999) 103–105.
[28] G. Rochat, Y. Leterrier, P. Fayet, J.-A.E. Månson, Influence of substrate additives on the mechanical properties of ultrathin oxide coatings on poly(ethylene terephthalate), Surf. Coat. Technol. 200 (2005) 2236–2242.
[29] J.L. Beuth, Cracking of thin bonded films in residual tension, Int. J. Solids Struct. 29 (1992) 1657–1675.
[30] E. Gumbel, Statistics of Extremes, Columbia University Press, NY, 1962.
[31] J.L. Beuth, N.W. Klingbeil, Cracking of thin films bonded to elastic–plastic substrates, J. Mech. Phys. Solids 44 (1996) 1411–1428.
[32] M.S. Hu, A.G. Evans, The cracking and decohesion of thin films on ductile substrates, Acta Metall. 37 (1989) 917–925.
[33] Y. Leterrier, D. Pellaton, J.-A.E. Månson, J. Andersons, Failure mechanics of thin coatings under multiaxial loading, in: A.H. Cardon, H. Fukuda, K.L. Reifsnider, G. Verchery (Eds.), Recent Developments in Durability Analysis of Composite Systems, Balkema, Rotterdam, 2000, pp. 29–35.
[34] Z. Chen, B. Cotterell, W. Wang, The fracture of brittle thin films on compliant substrates in flexible displays, Eng. Fract. Mech. 69 (2002) 597–603.
[35] G. Rochat, Y. Leterrier, P. Fayet, J.-A.E. Månson, Stress controlled gas-barrier oxide coatings on semi-crystalline polymers, Thin Solid Films 484 (2005) 94–99.
[36] Z. Chen, Z. Gan, Fracture toughness measurement of thin films on compliant substrate using controlled buckling test, Thin Solid Films 515 (2007) 3305–3309.
[37] M. Yanaka, Y. Kato, Y. Tsukahara, N. Takeda, Effects of temperature on the multiple cracking progress of sub-micron thick glass films deposited on a polymer substrate, Thin Solid Films 355–356 (1999) 337–342.
[38] A. Parvizi, K.W. Garrett, J.E. Bailey, Constrained cracking in glass fibre-reinforced epoxy cross-ply laminates, J. Mater. Sci. 13 (1978) 195–201.
[39] L. Boniface, P.A. Smith, M.G. Bader, A.H. Rezaifard, Transverse ply cracking in cross-ply CFRP laminates – initiation or propagation controlled?, J Compos. Mater. 31 (1997) 1080–1112.
[40] K.W. McElhaney, Q. Ma, Investigation of moisture-assisted fracture in SiO_2 films using a channel cracking technique, Acta Mater. 52 (2004) 3621–3629.